Molecular Crystals and Liquid Crystals

Publication details, including instructions for authors and subscription information:
http://www.tandfonline.com/loi/gmcl20

Doping and connecting carbon nanotubes

M. Terrones [a], N. Grobert [a], M. Terrones [b], H. Terrones [b], P. M. Ajayan [c], F. Banhart [d], X. Blase [e], D. L. Carroll [f], R. Czerw [f], B. Foley [f], J. C. Charlier [g], B. Foley [h], R. Kamalakaran [i], P. H. Kohler-Redlich [i], M. Rühle [i] & T. Seeger [i]

[a] Fullerene Science Centre, University of Sussex, Brighton, BN1 9QJ, UK

[b] IPICyT, Venustiano Carranza 2425-A, Col. Los Filtros, San Luis Potosí, SLP, 78210, México

[c] Department of Materials Science & Engineering, Rensselaer Polytechnic Institute, NY, USA

[d] Z. E. Elektronenmikroskopie, Universität Ulm, Ulm, 89069, Germany

[e] Département de Physique des Matériaux, Université Claude Bernard, Villeurbanne, 69622, France

[f] Department of Physics and Astronomy, Clemson University, Clemson, SC, 29634, USA

[g] Unit of Physics of Materials (PCPM), University of Louvain, Louvain-la-Neuve, 1348, Belgium

[h] Department of Physics, Trinity College Dublin, Dublin 2, Ireland

[i] Max-Planck-Institut für Metallforschung, Seestrasse 92, Stuttgart, D-70174, Germany

Version of record first published: 18 Oct 2010

Mol. Cryst. Liq. Cryst., Vol. 387, pp. [275]/51–[286]/62

1058-725X/02 $12.00 + .00
DOI: 10.1080/10587250290113556

DOPING AND CONNECTING CARBON NANOTUBES

M. Terrones and N. Grobert
Fullerene Science Centre, University of Sussex,
Brighton BN1 9QJ, UK

M. Terrones and H. Terrones
IPICyT, Venustiano Carranza 2425-A, Col. Los Filtros,
78210 San Luis Potosí, SLP. México

P. M. Ajayan
Department of Materials Science & Engineering,
Rensselaer Polytechnic Institute, NY-USA

F. Banhart
Z. E. Elektronenmikroskopie, Universität Ulm,
89069 Ulm, Germany

X. Blase
Département de Physique des Matériaux, Université Claude
Bernard, 69622 Villeurbanne, France

D. L. Carroll, R. Czerw, and B. Foley
Department of Physics and Astronomy,
Clemson University, Clemson SC 29634, USA

J. C. Charlier
Unit of Physics of Materials (PCPM), University of Louvain,
1348 Louvain-la-Neuve, Belgium

We are grateful to CONACYT-México grant W-8001-millennium initiative (HT, MT), AFOSR (DLC), the NSF (DLC), the AvH (MT), the Royal Society (NG), JFCC-Japan (NG), the Max-Planck-Gesellschaft (RK) and the DFG grant Ru342/11-2 (MR, PR, TS). JCC acknowledges the FNRS of Belgium and the Belgian Program on Inter-university Attraction Poles on Reduced Dimensionality Systems (PAI4/10). PMA acknowledges the NSF for supporting his research through the CAREER program. We are also grateful to S. Kühnemann, F. Philipp, H. Höschen and P. Kopold for electron microscopy support and technical assistance.

B. Foley
Department of Physics, Trinity College Dublin,
Dublin 2, Ireland

R. Kamalakaran, P. H. Kohler-Redlich, M. Rühle,
and T. Seeger
Max-Planck-Institut für Metallforschung, Seestrasse 92,
D-70174 Stuttgart, Germany

Self-assembly pyrolytic routes to arrays of aligned CN_x nanotubes are described. The electronic properties and the density of states (DOS) of these N doped tubes characterized by scanning tunneling spectroscopy (STS) are also presented. Using tight-binding calculations, we confirm that the presence of N is responsible for introducing donor states near the Fermi Level. Finally, it will be shown that high electron irradiation during annealing at 700–800°C, is capable of coalescing single-walled nanotubes (SWNTs). We investigate the merge at the atomic level using tight-binding molecular dynamics (TBMD). Vacancies induce the coalescence via a zipper-like mechanism, responsible of a continuous reorganization of atoms on individual tube lattices within the adjacent tubes. The latter results pave the way to the fabrication of nanotube contacts, nanocircuits and strong 3D composites using irradiation doses under annealing conditions.

Keywords: nanotubes; coalescence; doping; electronic; nanocircuits

INTRODUCTION

Carbon nanotube research has developed rapidly over the last decade. Recent examples of their applications [1] include use of nanotubes as: (i) gas storage components for Ar, N_2 [2] and H_2; (ii) STM probes and field emission sources; (iii) high power electrochemical capacitors; (iv) chemical sensors; (v) electronic nanoswitches; (vi) magnetic storage devices (e.g. Fe-filled nanotubes), etc [1].

In addition, other layered materials, analogues to graphite, such as BN [3], BC_2 [4], BC_3 [4], C_3N_4 [5–7] have been predicted to form nanotubes and other fullerene-like structures. Fortunately, some of these nanostructures (e.g. BN [8–11], BC_2N [12], BC_3[13,14], CN_x [15–18], MoS_2[19–20], WS_2 [21–2Z2], etc.) have been generated.

In this paper we discuss the produciton, structure and characterisation of CN_x nanotubes. The synthesis involves the pyrolysis of organometallic precursors such as ferrocene (biscyclopentadienyl-Iron) in conjunction

with melamine (triaminotriazine). The electronic properties of the tubular nanostructures were studied by STS. We also carried out molecular simulations, using tight binding methods, in order to confirm the results observed experimentally by STS.

Because of the outstanding electronic and mechanical properties of SWNTs, various applications in nano-electronics are envisaged. Nevertheless, an inherent problem associated with nanotubes lies in the difficulty in connecting them. Here, we also demonstrate that electron irradiation during annealing is capable of coalescing SWNTs [23]. The coalescence established between single-walled carbon nanotubes is studied, under electron irradiation at high temperature in a state-of-the-art transmission electron microscope. The process is finally investigated at the atomic level using exhaustive (TBMD) simulations. Vacancies induce the merge via a zipper-like mechanism within the adjacent tubes, which has been also observed experimentally.

N-DOPED CARBON NANOTUBES

The first report on the formation of aligned arrays of N-doped carbon nanotubes (<1–2%) involved the pyrolysis of aminodichlorotriazine over laser-etched Co thin films at 1050°C [24]. Unfortunately, this method liberated large number of N_2 molecules during thermolysis.

However, when melamine (triaminotriazine) is used as a CN precursor, higher nitrogen content (<7%) is observed within carbon tabular structures, which are also corrugated. In this particular case, aligned $C_{13}N_x$ ($x < 1$) nanotubes/nanofibers (<100 nm OD; <60 μm in length) can be produced by pyrolysing melamine over laser-etched Fe substrates [16,25]. The latter results demonstrate that it is not simple to produce highly ordered nanostructures containing large concentrations of N within the hexagonal carbon network.

Other alternative self-assembly processes have also been used to create large arrays ($<400 \times 400\ \mu m^2$) of aligned C_9N_x ($x \leq 1$) nanofibers (<100 nm OD, 60 μm length) using a ***single*** step process: ***e.g.*** the pyrolysis of ferrocene/melamine mixtures at 950–1050°C in an Ar atmosphere using a two stage furnace [16,25]. The overall morphology of the products exhibits a carpet-like structure, in which the doped tubes constitute the stack (Fig. 1).

High resolution transmission electron microscopy (HRTEM) studies reveal the presence of hollow nanofibers ("nanotubes") exhibiting irregular and interlinked corrugated morphologies (bamboo-like). It is important to note that the degree of perfection within the tubes decreases as a result of the nitrogen incorporation in the carbon lattice (Fig. 2). EEL spectra of the

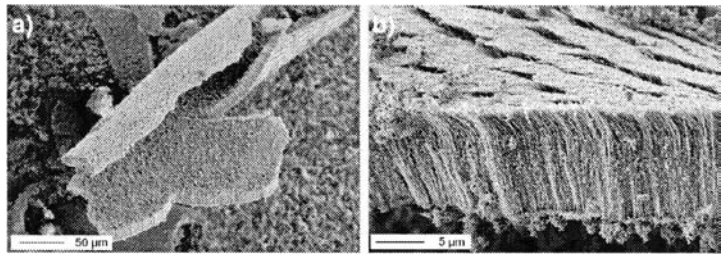

FIGURE 1 SEM images of: (a) a large flake (top view) containing aligned CN_x nanofibers; (b) higher magnification of a flake exhibiting densely packed fibers of uniform diameter (<60 nm OD).

doped nanofibers displayed ionization edges at *ca.* 284.5 eV and 400 eV corresponding to the C and N K-shells (Fig. 3a). A partition of the π^*-*type* peak of the nitrogen K-edge exhibits two prominent features located at *ca.* 398.7 and 400.7 eV (Fig. 3a). This splitting suggests two types of bonding of the N and C, within the hexagonal network. From the EEL spectra, it was estimated that the N content within the fibers was commensurate with C_9N_x ($x \leq 1$) stoichiometries.

XPS studies confirmed the N1s signal splitting at 398.7 eV and 400.9 eV (Fig. 3b). The binding energy centred at *ca.* 400.9 eV is attributed to highly coordinated N (N bonded to three C atoms), and the signal obtained at *ca.* 399 eV is commensurate with pyridinic nitrogen (N bonded to two C atoms). It is important to note that as the *overall* N content is raised within these

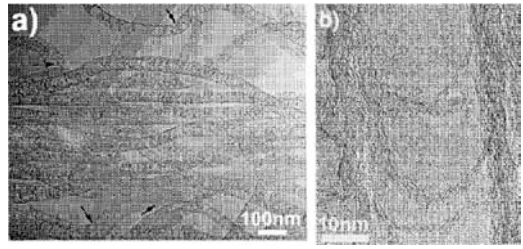

FIGURE 2 (a) TEM image of a typical region showing quasi-aligned N-doped carbon nanotubes. Their morphology consists of compartmentalized "stacked cones" (arrow indicate collapsed regions which do not break upon bending, thus they may behave as shock absorbing fillers in the fabrication of robust composites); (b) HRTEM image of a CN_x nanotube, exhibiting corrugation, interlinkage and compartments within an individual N-doped tubule.

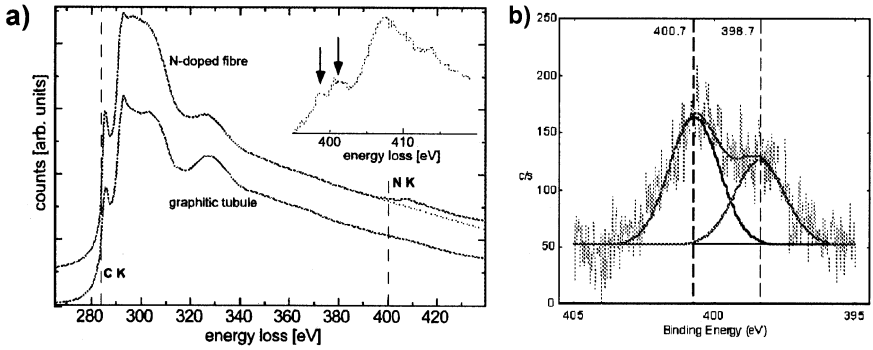

FIGURE 3 (a) EEL spectra of a typical C_xN_y nanotube compared to a pure carbon nanotube, suggesting an sp^2 graphite-like network due to the presence of the well defined π^* and σ^* features. Inset shows a splitting in the π^* of the NK-shell due to two different types of bonds; (b) N1s signal from the XPS spectrum of CN_x nanofibers revealing two peaks at *ca.* 398.7 eV and 400.9 eV.

tubules, the number of graphitic walls decrease and the proportion of pyridine-like N also increases (remaining almost constant the number of three coordinated N atoms). Therefore, we believe that these pyridine-like N "cavities" or "edges" embedded within the graphitic framework are responsible for interlinked morphologies observed in these N-doped carbon systems (Fig. 4).

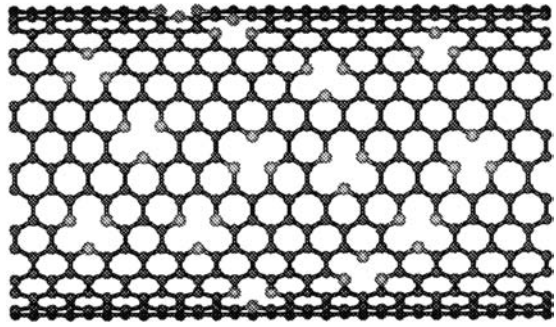

FIGURE 4 Molecular model of a CN_x nanotube containing pyridine-like N atoms. This model accounts for the 399 eV binding energy found experimentally by EELS and XPS studies.

ELECTRONIC PROPERTIES OF CN_x NANOTUBES

An STM image of a N-doped tube usually exhibit large holes or gaps (*ca.* 0.5–0.7 nm in diameter) within the lattice (circled regions in Fig. 5).

Figure 6 shows three typical ST spectra recorded within a straight section of a CN_x nanotube. For pure carbon nanotubes, the valence and conduction band features appear to be symmetric about the Fermi level [26–27], while for N-doped tubes (Fig. 6) an additional electronic feature occurs at *ca.* 0.18 eV. This result is in contrast to the B-doped case [26] where variations in the peak position are observed due to the creation of local phases, suggesting that N is distributed along the nanotube with small variations in the total N concentration. The presence of an electronic states at the Ef indicates that the N-doped material may also be metallic. In addition, this electron donor feature is always observed in our N-doped carbon material.

Because we observed the presence of pyridine-like sites by EELS and XPS, we carried out tight binding calculations using a recursion approach [28], which has proved successful for $B_xC_yN_z$ nanotube nanosystems [29]. In particular, we analysed the DOS associated with the N atoms arranged in a pyridinic fashion, randomly distributed within armchair and zigzag carbon nanotubes. The corresponding DOS for both types of chiralities are depicted in Figure 7. Here, it is clear the presence of prominent donor peaks close-above the Fermi energy (at *ca.* 0.2 eV), which are in good agreement with the experimental data obtained using STS (Fig. 6a). Thus, N doping, using

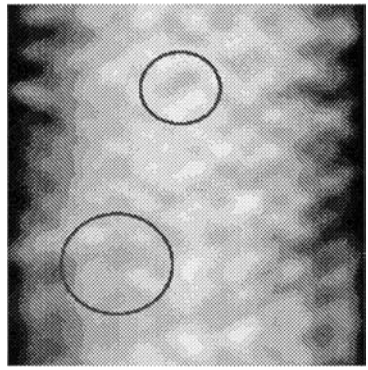

FIGURE 5 Atomic resolution STM image of the surface of a 20 nm diameter N-doped carbon nanotube exhibiting distortions and holes (circles), which are thought to be caused by the presence of pyridine-like islands (holes). Imaging of the tubes was recorded at a set point range of (500 mV at 20–500 pA). Images were acquired at room temperature.

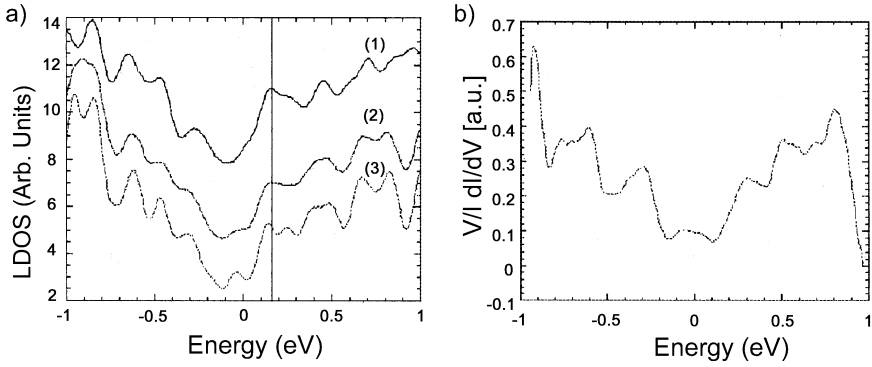

FIGURE 6 (a) Tunneling spectra recorded on a clean section of an N-doped carbon nanotube. Spectra (1)–(3) were taken at different locations along the surface but close to a "hole" as shown in Figure 5. Note the peak at 0.18 eV in all spectra; (b) Tunneling spectra of a pure MWNT of 20 nm. Notice the regularly spaced van Hove singularities signifying the one-dimensional nature of the material. All spectra were converted to the corresponding LDOS using the Feenstra algorithm of numerical differentiation and normalization for the STM tip height (dI/dV)/(I/V).

pyridine-type units within carbon tubes, are responsible for a strong related π peak (shown by arrows in the black curves of Fig. 7) in the conduction band of the original undoped carbon nanotube (red curves, Fig. 7).

COALESCENCE OF SINGLE-WALLED NANOTUBES

A time resolved sequence of the coalescence process observed within a SWNT bundle (produced by the arc technique), in which the merger of tubes takes place over a relatively long time period is shown in Figure 8. In the beginning, two of the outer tubes establish a 'link' in a dumbbell-like configuration (Fig. 8c). Subsequently, the joined tubes coalesce into a larger tube of nearly double the cross section. Finally, the coalesced nanotube reaches a metastable geometry (Fig. 8f). Such process is frequently observed at the edge of the bundle, probably because free space among tubes is needed to establish the merger.

In order to investigate the nanotube coalescence, we have performed TBMD calculations involving an energy functional and a parameterisation for modelling various carbon allotropes [23]. These calculations involve two adjacent (10,10) nanotubes, containing random vacancies and dangling bonds (Fig. 9), along the nearest-neighboring edge. The simulation starts with the creation of 20 vacancies in two adjacent nanotubes (contained in a

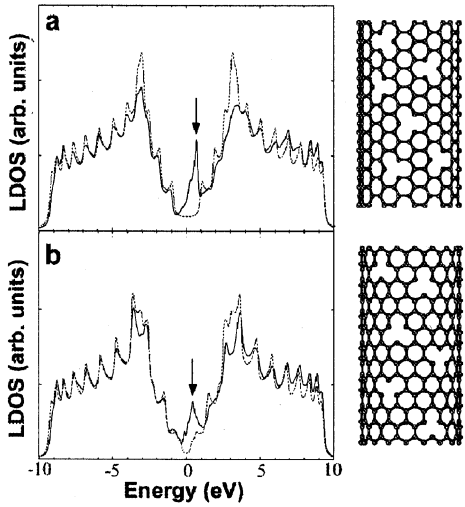

FIGURE 7 Theoretical LDOS of CN_x nanotubes containing pyridine-like structures (a) armchair (10,10) and (b) zigzag (17,0) configuration. In both cases, N atoms were placed randomly (N: red spheres – C: blue spheres; right hand images). The LDOS of doped (black curve) and pure (red curve) carbon nanotubes are compared. It is clear that pyridine-like sites are responsible for the prominent donor-like features (shown by arrows in the conduction band) close-above the Fermi energy. Note that the semiconducting (zigzag) nanotube becomes metallic after introducing N in the carbon lattice.

820 atom unit cell; Fig. 9a). It is noteworthy that the number of vacancies is only about 2.5% of defects within the cell, which can be easily produced in our irradiation experiments (under the conditions of the present experiment, each carbon atom is displaced approximately every 100 seconds). These TBMD calculations were carried out within a total simulation time of 150 ps. After 100 ps, a connection between the two tubes was established (Fig. 9b), similar to the dumbbell shape observed experimentally in Figure 8c, and a zipper-like mechanism proceeded to anneal the structures. Figure 9c reveals that the tubes have coalesced after 150 ps into a larger tubule of about 2.6 nm diameter. The coalesced tube consists of nearly pure sp^2 hexagonal framework (Fig. 9).

Figure 10 confirms the existence of zipping mechanism. In this case two nanotubes (under the same condition of irradiation and temperature) lying along their axis and very close to each other, can be distinguished. After 1–3 min, the tubes start to coalesce (bottom left Fig. 10b) into one of larger diameter (Fig. 10c). The zipping can be witnessed by the presence of dark contrast indicated by the arrow in Figure 10c. Finally, the tubes merge into

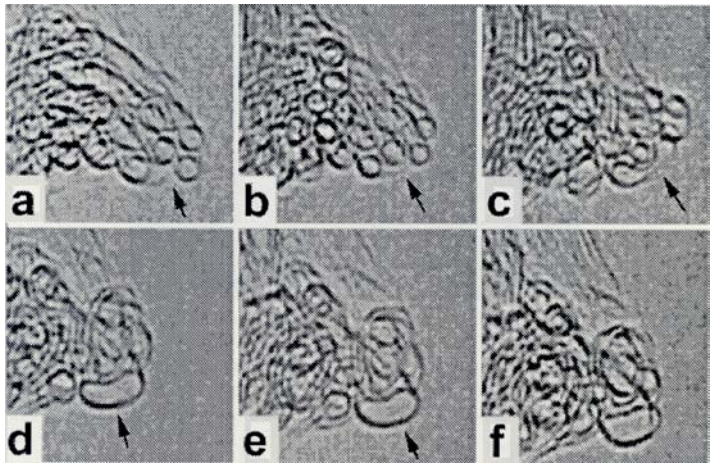

FIGURE 8 HRTEM images of the coalescence process observed within a bundle of SWNT's: (a–b) cross-sections of four nanotubes are clearly observed; c) Two of the outer nanotubes link and establish a sort of 'belt' in a dumbbell fashion; (d–e) the tubes coalesce into a rounder cross-section, and (f) the coalesced tubes reach a metastable state. SWNT bundles were produced using Ni–Y catalysts in a carbon arc apparatus. Bulk SWNTs were then placed onto cupper TEM grids. The grids were inserted in a 1.25 MeV Atomic Resolution Transmission Electron Microscope (ARTEM; Joel-ARM 1250 located at the Max-Planck-Institut für Metallforschung in Stuttgart, Germany) equipped with a heating stage. All experiments were conducted at specimen temperatures of 700–800°C.

a single tube of large diameter (Fig. 10d). This image confirms that the zipping mechanism should always take place during nanotube coalescence.

It is believed that electron irradiation removes carbon atoms from the nanotube(s) lattice by knock-on displacements. The high temperature experienced by the tubes in our experiments guarantee a high mobility of interstitials and fast annealing of defects. Due to the presence of dangling bonds produced by radiation, vacancies are induced. Therefore, the irradiated tube(s) will establish links in order to satisfy most of the dangling bonds. This coalescence phenomenon should also be driven by strain energy minimization so that more stable tubes of larger diameter are created.

Therefore, nanotube coalescence should involve various phenomena that occur almost simultaneously: (a) defect formation or the presence of reactive sites (*e.g.* vacancies, interstitials, dangling bonds); (b) surface and atom reconstruction initiated by electron irradiation; and (c) thermal annealing (zipping). We believe that coalescence of tubes of different chiralities will not take place because a large number of rearrangements of

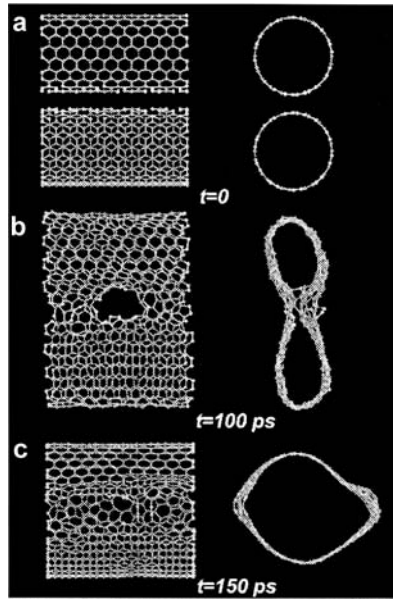

FIGURE 9 Sequences of coalescence obtained using TBMD simulations (side and cross-section views) between two adjacent (10,10) carbon nanotubes (diameter: 1.36 nm). After coalescence the reconstructed surface exhibits some remaining vacancies (dangling bonds), but the time scale of our simulation prevented us from studying further the evolution of the process (two-coordinated atoms in green, four-coordinated in red — only one).

atoms needs to occur along the tube lattice. However, local polymerization should result under such conditions [23]. We believe that controlled irradiation should be able to generate fascinating molecular interconnections such as Y-junctions, T-junctions and nanotube joints.

CONCLUSIONS

It is possible to fabricate n-type carbon nanotubes using nitrogen as a doping agent. The tubes can be synthesised using various pyrolytic techniques, however we consider that the pyrolysis of ferrocene/melamine mixtures 900–1050°C in the presence of Ar is the best way to generate large arrays of CN_x nanotubes. We have also confirmed the existence of donor states using STS, STM and TB calculations. Finally, we have observed (in-situ) the coalescence of SWNTs under high electron irradiation at high temperatures. In this context, we have elucidated the mechanism whereby nanotubes merge into tubules of larger diameter. This

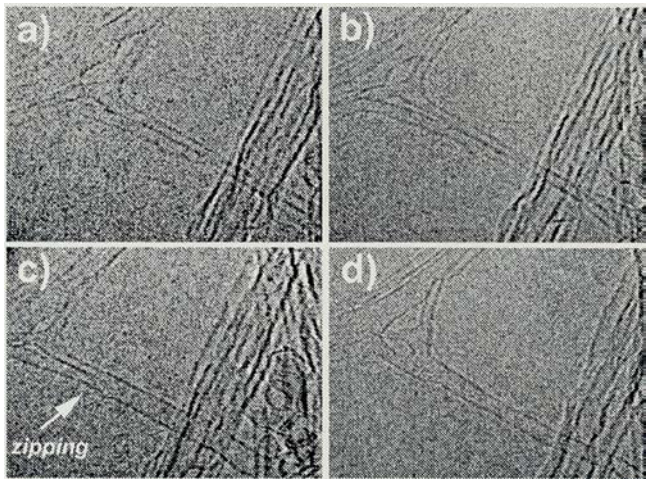

FIGURE 10 Sequence for the zipping mechanism witnessed during the coalescence of two SWNTs. HRTEM images of the tubes prior to coalescence (a). As irradiation and high temperature continue, the tubes get closer (b). Subsequently, these tubes start to coalesce into one and the zipping is confirmed by the presence of an intersection of 3 and two dark lines (see arrow in c). Finally the tubes coalesce into one of larger diameter (d). Tube narrow diameter is *ca.* 1.2–1.4 nm.

phenomenon consists of the creation of vacancies, which trigger the reconstruction of the tube surfaces, thus forming a more stable tubule of large diameter. The latter result implies that it should be possible to fabricate "T" and "Y" junctions as well as carbon tube networks, which will certainly revolutionise key areas in nanotechnology.

REFERENCES

[1] Terrones, M., Hsu, W. K., Kroto, H. W., & Walton, D. R. M. (1998). In *Fullerenes and Related Structures*: Topics in Chemistry Series, Hirsch (Ed.), Vol. 199, Ch. 6 (pp. 189–234), Springer-Verlag.
[2] Terrones, M., Kamalakaran, R., Seeger, T., & Rühle, M. (2001). *Chem. Commun.*, *23*, 2335–2336.
[3] Blase, X., Rubio, A., Louie, S. G., & Cohen, M. L. (1994). *Europhys. Lett.*, *28*, 335–340.
[4] Miyamoto, Y., Rubio, A., Cohen, M. L., & Louie, S. G. (1994). *Phys. Rev. B*, *50*, 4976–4979.
[5] Liu, A. Y. & Cohen, M. L. (1989). *Science*, *245*, 841–842.
[6] Teter, D. M. & Hemley, R. J. (1996). *Science*, *271*, 53–55.
[7] Miyamoto, Y., Cohen, M. L., & Louie, S. G. (1997). *Solid State Commun.*, *102*, 605–608.
[8] Chopra, N. G., Luyken, R. J., Cherrey, K., Crespi, V. H., Cohen, M. L., Louie, S. G., & Zettl, A. (1995). *Science*, *269*, 966–967.
[9] Loiseau, A., Willaime, F., Demoncy, N., Hug, G., & Pascard, H. (1996). *Phys. Rev. Lett. 76*, 4737–4740.

[10] Terrones, M., Hsu, W. K., Terrones, H., Zhang, J. P., Ramos, S., Hare, J. P., Castillo, R., Prassides, K., Cheetham, A. K., Kroto, H. W., & Walton, D. R. M. (1996). *Chem. Phys. Lett.*, *259*, 568–573.
[11] Golberg, D., Bando, Y., Eremets, M., Takemura, K., Kurashima, K., Tamiya, K., & Yusa, H. (1997). *Chem. Phys. Lett.*, *279*, 191–196.
[12] Terrones, M., Benito, A. M., Manteca-Diego, C., Hsu, W. K., Osman, O. I., Hare, J. P., Reid, D. G., Terrones, H., Cheetham, A. K., Prassides, K., Kroto, H. W., & Walton, D. R. M. (1996). *Chem. Phys. Lett.*, *257*, 576–582.
[13] Sen, R., Satishkumar, B. C., Govindaraj, A., Harikumar, K. R., Raina, G., Zhang, J. P., Cheetham, A. K., & Rao, C. N. R. (1998). *Chem. Phys. Lett.*, *287*, 671–676.
[14] Terrones, M., Hsu, W. K., Ramos, S., Castillo, R., & Terrones, H. (1998). *Full. Sci. & Tech.*, *6*, 787–800.
[15] Sen, R., Satishkumar, B. C., Govindaraj, S., Harikumar, K. R., Renganathan, M. K., & Rao C. N. R. (1997). *J. Mater. Chem.*, *12*, 2335–2337.
[16] Terrones, M., Redlich, Ph., Grobert, N., Trasobares, S., Hsu, W. K., Terrones, H., Zhu, Y. Q., Hare, J. P., Cheetham, A. K., Rühle, M., Kroto, H. W., & Walton, D. R. M. (1999). *Adv. Mater.*, *11*, 655–658.
[17] Terrones, M., Terrones, H., Grobert, N., Hsu, W. K., Zhu, Y. Q., Kroto, H. W., Walton, D. R. M., Kohler-Redlich, Ph., Rühle, M., Zhang, J. P., & Cheetham. A. K. (1999). *Appl. Phys. Lett.*, *75*, 3932–3934.
[18] Suenaga, K., Yudasaka, M., Colliex, C., & Iijima, S. (2000). *Chem. Phys. Lett. 316*, 365–372.
[19] Tenne, R., Margulis, L., Genut, M., & Hodes, G. (1992). *Nature*, *360*, 444–446.
[20] Hsu, W. K., Chang, B. H., Zhu, Y. Q., Han, W. Q., Terrones, H., Terrones, M., Grobert, N., Cheetham, A. K., Kroto, H. W., & Walton, D. R. M. (2000). *J. Am. Chem. Soc.*, *122*, 10155–10158.
[21] Margulis, L., Saltra, G., Tenne, R., & Tallanker, M. (1993). *Nature*, *365*, 113–114.
[22] Zhu, Y. Q., Hsu, W. K., Grobert, N., Chang, B. H., Terrones, M., Terrones, H., Kroto, H. W., Walton, D. R. M., & Wei, B. Q. (2000). *Chem. Mater.*, *10*, 2570–2577.
[23] Terrones, M., Terrones, H., Banhart, F., Charlier, J. C., & Ajayan, P. M. (2000). *Science*, *288*, 1226–1229.
[24] Terrones, M., Grobert, N., Olivares, J., Zhang, J. P., Terrones, H., Kordatos, K., Hsu, W. K., Hare, J. P., Townsend, P. D., Prassides, K., Cheetham, A. K., Kroto, H. W., & Walton, D. R. M. (1997). *Nature*, *388*, 52–55.
[25] Grobert, N., Terrones, M., Trasobares, S., Kordatos, K., Terrones, H., Olivares, J., Zhang, J. P., Redlich, Ph., Hsu, W. K., Reeves, C. L., Wallis, D. J., Zhu, Y. Q., Hare, J. P., Pidduck, A. J., Kroto, H. W., & Walton, D. R. M. (2000). *Appl. Phys. A-Mater. Sci. & Process.*, *70*, 175–183.
[26] Carroll, D. L., Redlich, Ph., Blase, X., Charlier, J. C., Curran, S., Ajayan, P. M., Roth, S., Rühle, M. (1998). *Phys. Rev. Lett.*, *81*, 2332–2335.
[27] Czerw, R., Terrones, M., Charlier, J. C., Blase, X., Foley, B., Kamalakaran, R., Grobert, N., Terrones, H., Tekleab, D., Ajayan, P. M., Blau, W., Rühle, M., & Carroll, D. L. (2001). *Nanoletters*, *1*, 457–460.
[28] Haydock, R., Heine, V., & Kelly, M. J. (1972). *J. Phys. C.*, *5*, 2845.
[29] Blase, X., Charlier, J. C., DeVita, A., & Car, R. (1997). *Appl. Phys. Lett.*, *70*, 197.